Bitbow: a digital format of Brainbow enables highly efficient neuronal lineage tracing and morphology reconstruction in single brains

Ye Li[1], Logan A Walker[2], Yimeng Zhao[1], Erica M Edwards[1], Nigel S Michki[2], Hon Pong Jimmy Cheng[1], Marya Ghazzi[1], Tiffany Y Chen[1], Maggie Chen[1], Douglas H Roossien[1], Dawen Cai[1,2,3]

1 Department of Cell and Developmental Biology, University of Michigan Medical School
2 Biophysics, University of Michigan School of Literature, Science, and the Arts
3 Neuroscience Graduate Program, University of Michigan Medical School
Corresponding: Dawen Cai <dwcai@umich.edu>

Abstract

Identifying the cellular origins and mapping the dendritic and axonal arbors of neurons have been century old quests to understand the heterogeneity among these brain cells. Classical chemical and genetic methods take advantage of light microscopy and sparse labeling to unambiguously, albeit inefficiently, trace a few neuronal lineages or reconstruct their morphologies in each sampled brain. To improve the analysis throughput, we designed Bitbow, a digital format of Brainbow which exponentially expands the color palette to provide tens of thousands of spectrally resolved unique labels. We generated transgenic Bitbow *Drosophila* lines, established statistical tools, and streamlined sample preparation, image processing and data analysis pipelines to allow conveniently mapping neural lineages, studying neuronal morphology and revealing neural network patterns with an unprecedented speed, scale and resolution.

Introduction

Bilaterian nervous systems are built upon heterogeneous populations of neurons that form interconnected circuits. To understand the molecular and cellular mechanisms that lead to proper circuit formation, it is critical to elucidate the lineage origin and morphology formation of neurons. This is because lineages mark the outcome of neurogenesis, while morphology dictates the circuit structure by defining physical boundaries of the receptive and projective fields. Tremendous efforts have been made in the past century to take on these two fundamental quests in neuroscience, evolving from methodologies that can cope with one or a few neurons at a time, such as stochastic silver staining (Golgi's method)[1,2] and mosaic genetic labeling[3,4], to multispectral labeling technologies (Brainbow) that can differentiate large population of neurons in the same tissue[5].

Brainbow and Brainbow-like tools label neurons in distinct colors by expressing random ratios of different fluorophores, such as fluorescent proteins (FPs), upon genome recombination[6–8]. Reagents, including mice[5,9,10], fruit flies[11–17], zebrafish[18–21], bacteria[22], and viruses[10,23–25] are now broadly available for lineage and morphology studies. In lineage studies, unique colors generated in the progenitor cells and inherited by their progenies were used to depict the clonal expansion process of adjacent lineages[9,15,19,26,27]. In morphology studies, the unique colors of neurites aided in identification of parallel projection patterns[21,28] and confirming presynaptic inputs from multiple neurons converging to a common target[29–32]. However, current designs are often limited to generating up to tens of reliably distinguishable colors in a transgenic animal. The small unique color pool results in a high probability of labeling neighboring cells with the same color, therefore constraining the labeling density for neuronal morphology reconstructions. This makes it even more challenging to interpret lineage tracing results due to the need for unique colors to specify cells in the same lineage. In addition, distinguishing color variants differing by intensity levels in spectral channels is not reliable for lineage tracing because FP expression level may vary among cells in the same lineage.

One way to generate more unique labels for lineage tracing is to localize the same FPs to different subcellular compartments. In strategies such as CLoNe and MAGIC, Brainbow cassettes targeted to cytoplasm, cell membrane, nucleus, and/or mitochondria were co-electroporated with transposase for genome integration, which allowed the differentiation of neighboring progenies in chick and mouse embryos with fewer color collisions[26,27]. However, the number of expression cassettes being integrated in each cell is random in these experiments, leading to uncertainty in each color's appearance probability which complicates quantitative analysis. The Raeppli strategy solves this problem by generating a transgenic *Drosophila* which utilizes 4 FPs to create up to 4 x 4 = 16 membrane and nucleus color combinations[16]. In parallel, strategies such as TIE-DYE and MultiColor FlpOut (MCFO) attempt to generate more color combinations by stochastically removing the expression stops from each

FP module [15,28]. While inserting 3 different modules into 3 genomic loci allows generating up to 2^3-1=7 unique labels, it is difficult to insert more modules to more genomic loci in a single transgenic animal.

Here we present Bitbow, a digital format of Brainbow to greatly expand the unique color pool from a single transgenic cassette. Unlike the original Brainbow, whose FP choices are exclusive in one cassette, Bitbow allows each FP to independently express in an ON or OFF state upon recombination. Color coding by each FP's binary status is similar to the information coding by each bit in computer memory, thus leading to the name Bitbow. In a recent study, we implemented the Bitbow1 design to target 5 spectrally distinct FPs to the nucleus for lineage tracing[33]. Here, we present novel Bitbow1 flies which encode up to 32,767 unique "colors" (Bitbow codes) in a single transgenic animal. This allows reliable lineage tracing without complicated statistical tests[33]. To better enable morphology tracing, we generated Bitbow2, which couples Bitbow1 to a self-regulating recombination mechanism. This enables generating consistent neuronal labeling by a simple cross of a Bitbow2 fly to an enhancer-Gal4 driver fly without the need for heat-shock.

Results

Characterization of Bitbow design in the *Drosophila* brain

To permit independent recombination of each FP, we utilized a pair of inverted FRT sites flanking a reversely positioned FP. downstream of a 10xUAS sequence and upstream of a polyadenylation sequence (**Fig. 1a**). This default OFF state guarantees a non-fluorescent expression. Upon Flp recombination, the flanked FP spins between the inverted FRT sites, resulting in either an ON or OFF state of expression driven by Gal4. Such a design exponentially increases the color-coding capacity with increasing numbers of bits (FPs) in the same transgenic animal (**Fig. 1b**), however, requires a transient Flp activity to ensure the recombination choice is stabilized, similar to the original Brainrow2 design[5]. In order to guarantee independent recombination between each FP, we used incompatible flanking FRT sequences. Other than the three previously-used incompatible Frt sites[10], FRT-F3, FRT-5T2, and FRT-545, we identified FRT-F13, FRT-F14, and FRT-F15 as additional incompatible sites in a screen (**Fig. S1**)[34]. As FRT-F15 has lower recombination efficiency (data not shown), we ended up with a 5-bit Bitbow1.0 design that consists the other 5 FRT sites to control the independent recombination choices of mAmetrine, mTFP1, mNeonGreen, mKusabira-Orange2 and tdKatushaka2, respectively[35–39]. These FPs were chosen for their brightness, photo-stability, antigenicity, and spectral separation (**Fig. S2**). Finally, we made the cell membrane-targeting Bitbow1.0 (mBitbow1.0) fly to better reveal whole neuron morphology.

Next, we crossed mBitbow1.0 flies to hsFlp;;elav-Gal4 driver flies to examine the offspring expression in the nervous system upon heat-shock induced transient Flp activity. When young adult offspring were heat-shocked at 1 day after eclosion and imaged at 3 days later (**Fig. 1c**),

we observed individual neurons expressing unique combinations of Bitbow codes that can be denoted as a series of 5-bit 0/1 digits (**Fig. 1d**, **1e**). Increasing the number of heat-shocks (thus Flp activity) increased the total number of neurons being labeled and the number of FP species being expressed in each neuron (**Fig. S3**). Nonetheless, all 31 expected Bitbow codes were identified, albeit each of which was observed with a different frequency (**Fig. S4**). The appearance of strong and diverse Bitbow code labeling days after transient heat-shock also indicated that recombination outcomes induced by transient Flp activity were stable. Otherwise, all FPs would keep spinning so that they would all have some transcripts positioned in the forward direction to become fluorescent in all cells.

Depending on the timing of heat-shock, stochastic colors can be observed in neighboring neurons or clusters of neuronal progenies if recombination happens in postmitotic neurons or progenitor cells, respectively[26]. While post-eclosion heat-shock demonstrated the former situation, the later situation can be examined by heat-shocking at 24 hours after egg laid (24hr AEL, i.e., early 1st instar larval stage) and imaging at 72 hours post heat-shock, at the 3rd instar larval stage (**Fig. 1f**). Interestingly, while there are plenty of postmitotic neurons at the 1st instar larval stage, most neighboring neurons were labeled as cell clusters in the same Bitbow code (**Fig. 1g**). In addition, we always observed a much larger size neuroblast (NB, i.e., neural stem cell) being labeled in the same Bitbow code in each cluster (**Fig. 1g inset**, asterisk). Collectively, these observations suggested that under the heat-shock conditions optimized for larvae survival, recombination events mostly happened in the NBs and the recombination outcome did not change over time. Quantification of the expression frequency of each FP, i.e., the recombination rate of each FRT site, indicates that FRT-545 has the highest recombination rate, followed by FRT-F3, and FRT-5T2, while FRT-F14 and FRT-F13 have the similarly lowest among the five (**Fig. 1h**). This observation is not specific to the membrane targeting, but is consistent in other Bitbow1.0 flies (**Fig. S5** and detailed below).

Targeting Bitbow FPs to multiple subcellular compartments permits high-throughput lineage tracing in the whole *Drosophila* brain without ambiguity

In a recent study, we specified the lineage relationships between pairs of *Drosophila* peripheral neurons using a nucleus-targeting Bitbow1.0 (nBitbow1.0) that can generate 31 unique Bitbow codes[33]. However, many more unique Bitbow codes are needed to unambiguously label the ~200 neuronal lineages in the *Drosophila* central brain. We made a membrane/nucleus double-targeted mnBitbow1.0 fly and an additional Golgi apparatus triple-targeted mngBitbow1.0 fly (**Fig. 2a**) to generate up to 1023 and 32,767 (**Fig. 2b**) unique Bitbow codes in the same brain, respectively.

To examine the labeling efficacy, we crossed mnBitbow1.0 or mngBitbow1.0 flies to hsFlp;;elav-Gal4 flies, and performed the larval heat-shock experiment (**Fig. 2c**) to their offspring (**Fig. S5**, or **Fig. 2d**, respectively). As expected, we identified many cell clusters, in

133 which all the cells were labeled by the same combinatorial Bitbow code (**Fig. 2d-2f**), which
134 again indicated the transient Flp activity led to stable recombination outcome in the neural
135 stem cells. Many of these Bitbow codes contain FPs in more than one subcellular
136 compartments, which indicates that the repeated incompatible FRT sites inserted in distant
137 chromosome locations are exempt from inter-Bitbow cassette recombination. In addition,
138 these subcellular compartments are spatially well separated, even when the same FPs are
139 expressed in different subcellular compartments in the same cell (**Fig. 2f**).
140 To estimate the theoretical ability to unambiguously distinguish Bitbow flies' 200 lineages in
141 the same *Drosophila* central brain, we ran a simulation to calculate how frequently the same
142 Bitbow codes are seen in more than one lineage, i.e. the collision rate. The simulation shows
143 that there would be a 84.5%, 9.1%, or 0.3% collision rate in a Bitbow fly that targets the 5 FPs to
144 1, 2, or 3 subcellular compartments, corresponding to 5-bit, 10-bit, or 15-bit Bitbow codes,
145 respectively (**Fig. 2g** blue, green or red dashed lines, respectively). In other words, under
146 uniformly random recombination conditions, we can identify any neuron's lineage composition
147 in the mngBitbow1.0 fly central brain with 99.7% confidence. To estimate the collision rate in
148 real experiments, we conducted the early heat-shock experiment as shown in **Fig. 2c** with
149 mnBitbow1.0 or mngBitbow1.0 flies. We plotted the percentages of cell clusters that are
150 uniquely labeled, or 2 of them, or >=3 of them are labeled by the same Bitbow code in each
151 brain. We found that the experimental collision rates of mnBitbow and mngBitbow fly brains
152 are 69.8%±5.7% (mean±SD, 286 clusters from 4 brains) and 51.1%±8.5% (mean±SD, 577 clusters
153 from 6 brains), respectively (**Fig. 2h**).
154 It seems desperate that the high collision rate would make even the mngBitbow1.0 fly
155 useless for tracing neuronal lineages in the *Drosophila* central brain. However, we have shown
156 that it is possible to develop a novel statistical method and apply it to the nBitbow1.0 flies to
157 determine the lineage relationships between any two neighboring neurons in the *Drosophila*
158 PNS[33]. Given that the mngBitbow1.0 fly generates much more unique Bitbow codes, we sought
159 a different strategy to simplify the analysis yet ensure proper statistical power to
160 unambiguously trace any neuronal lineage composition in the *Drosophila* central brain. We
161 plotted the percentages of Bitbow codes that are expressed in 1, or 2, or >=3 clusters in each
162 brain (**Fig. 2i**). We found that the majority of labeling collisions were contributed by a small
163 number of Bitbow codes, most among which have mNeonGreen being turned on (**Fig. S6**). To
164 estimate the effect of the FP turn-on bias to the apparent Bitbow code collision rates, we
165 quantified the relative recombination frequencies of the incompatible FRT sites in
166 mngBitbow1.0 (**Fig. S7a**), calculated the empirical frequencies of all 32,767 mngBitbow codes
167 (**Fig. S7b**), and used the empirical frequencies to run the same simulation as shown above (**Fig.
168 2g**). We found that mngBitbow1.0's experimental collision rate was estimated as 40.3% for 200
169 lineages (**Fig. 2g** green solid line), and a small number of codes appeared much more
170 frequently, which contributed to most of the high collision events (**Fig. S7c**). Next, we excluded

171 the most frequent 67 or 767 mngBitbow codes from the simulation and found the collision rate
172 was decreased to 14.3% or 4.6%, respectively (**Fig. 2g**, orange, and purple solid lines). In other
173 words, we have over 85.7% or 95.4% confidence to call any neurons belonging to the same
174 lineage using the pool of 32,700 or 32,000 unique mngBitbow codes, respectively.
175 Encouraged by mngBitbow's potential in determining lineage relationships with high
176 confidence, we ran another simulation to estimate the number of animals needed to
177 thoroughly survey the lineage relationship of any Gal4-driver labeled neurons across the whole
178 central brain, i.e. every one of the 200 lineages needs to be observed at least once (**Fig. 2j**). We
179 included the estimation for the popular method MARCM as a comparison[3]. In the simulation,
180 we assumed a 48.08% lineage coverage for mngBitbow1.0 (577 clusters observed from six
181 central brains containing an estimated total of 1200 neuronal lineages) and a 1% lineage
182 coverage for MARCM to make sure no more than one lineage being labeled in each brain. This
183 assumption underestimates the animal used in real MARCM experiments, that is because the
184 same clonal patterns are normally required to be repeated more than once to confirm the
185 labeling is indeed unique. Our simulation matches well with previous MARCM experiments [40–
186 42], in which hundreds to thousands of brains were needed in one experiment (**Fig. 2j**, cyan line).
187 Using mngBitbow1.0, only 28.3±6.4 flies (mean±SD) were needed to survey each of the 200
188 lineages at least once while achieving an overall >85% confidence in determining the lineage
189 relationship between any neurons (**Fig. 2j**, orange line).
190 Next, we set out to use mngBitbow1.0 to determine the lineage relationships of serotonergic
191 neurons in the *Drosophila* CNS. Serotonergic neurons are a group of ~100 neurons that have
192 been shown to play critical roles in maintaining and regulating important neural functions in the
193 fly, such as feeding, courtship, aggression, learning and memory[43–48]. Born in late embryonic
194 stages, serotonergic neurons persist through larval, pupal and adult stages and form
195 stereotypical clusters across the brain, especially in each hemi-segment of the ventral nerve
196 cord (VNC, **Fig. 3a**)[49]. However, whether the serotonergic neurons in the same cluster originate
197 from the same neural stem cell has not been experimentally determined. We crossed
198 mngBitbow1.0 flies to hsFlp;TRH-Gal4; flies, heat-shocked the offspring embryos in an early
199 neurogenesis period (0-4 hrs AEL), and imaged the serotonergic neurons in 3rd instar larva (**Fig.
200 3b**). We observed that all serotonergic neurons clustered in each hemi-segment of the VNC or
201 in the central brain were labeled by distinct Bitbow codes (**Fig. 3c-3e**, **Fig. S8**), except on one
202 occasion that two out of the four SE0 neurons near the esophagus hole were labeled by a
203 Bitbow code of high collision rate (**Fig. S8**). We believe that the observation of adjacent
204 serotonergic neurons being labeled in distinct Bitbow codes is not due to embryonic heat-
205 shock, because in the control experiment utilizing a hsFlp;elav-Gal4; fly, many cell clusters
206 labeled in the same Bitbow codes were observed (**Fig. S9**). In summary, our Bitbow study
207 indicated that the majority of serotonergic neurons arise from distinct lineages.

Bitbow2 enables broad neuron morphology labeling with a simple transgenic setup

While inducing Flp expression by heat-shock has the flexibility in controlling the timing of Bitbow1.0 recombination for lineage tracing, the relatively low Flp activity resulted in reduced color variation and labeling coverage, which constrains tracing morphology of postmitotic neurons (**Fig. S3**). Increasing heat-shock duration to increase Flp activity was not ideal, because the animals were challenged by stronger stress, which resulted in a lower survival rate (data not shown). In addition, the requirement of heat-shocks limited the use of Bitbow in combination with other temperature-dependent interrogations[50,51]. Finally, the hsFlp/enhancer-Gal4/Bitbow triple transgenes are more complicated to set up.

To overcome the above-mentioned limitations, we designed Bitbow2, in which a self-regulating Flp (srFlp) is added to Bitbow1 (**Fig. 4a**). The srFlp consists of a flippase cDNA flanked by a pair of FRT sites positioned in the same direction. Driven by the promoter of *Drosophila* neuronal Synaptobrevin (nSyb)[52], this design permits a strong burst of neuronal-specific expression of flippase which recombines the FP modules to generate Bitbow codes and eventually excises out the flippase cDNA to prevent chromosome breaks caused by excessive recombination. To ensure sufficient amount of flippase being produced before its coding sequence being removed, we made mBitbow2.0 and mBitbow2.1, which utilized the less efficient FRT-F13 and FRT-F15 sites to lower the chance of self-excision, respectively.

To compare the labeling coverage of Bitbow1 and Bitbow2 flies, we again used the TRH-Gal4 fly to constrain labeling in ~100 neurons across the whole larva brain (**Fig. 4b**, **4c**). As expected, we found that Bitbow2.1 had the best labeling coverage, as high as 93.8% in the flies that carried two copies of the transgene (**Fig. 4d**). We also found that colorful Bitbow2 labeling could be achieved by direct crosses to various subtype specific enhancer-Gal4 driver lines (**Fig. 5e** and **Fig. S10**). Finally, when crossing a Bitbow2.1 fly to an elav-Gal4 fly, its offspring labeled neighboring neurons labeled in many distinct Bitbow colors, which indicates that Flp recombination is specific in postmitotic neurons (**Fig. 5f**). Again, the diverse Bitbow colors indicated the srFlp activity is strong yet transient to ensure stable recombination outcomes.

Bitbow2 enables neural anatomy and network analysis in the *Drosophila* central nervous system

As Bitbow2 provides rich color and broad coverage labeling, we expect it can be used to simultaneously resolve many neuron morphologies in the same brain. This not only increases the experimental throughput, but also eliminates the sampling errors and animal-to-animal variations in experiments that rely on aligning sparsely reconstructed neurons from multiple brains to a common reference[53]. To gain higher imaging resolution to resolve the intermingled neurites in the dense neuropil, we applied a modified protein-retention Expansion Microscopy (proExM) protocol to the Bitbow2 *Drosophila* brain (**Fig. S11**)[54–56]. With ~4x expansion, we could use nTracer[31] to reconstruct all 21 Bitbow-labeled (out of 26 estimated total [46,56]) VNC serotonergic neurons from the A2 to A8/9 segments of a single 3rd instar larva brain (**Fig. 5a**

246 and **Movie S1, S2**). We sampled the Bitbow colors along the somas and processes of these
247 neurons and found these 21 neurons were labeled by 16 well-separated colors in a UMAP
248 projection (**Fig. S12a**). Although there were 3 unique Bitbow colors, each of which labeled 2, 2,
249 or 4 neurons, their subtle color differences (**Fig. S12b**) and well-separated physical locations
250 (**Fig. S12c**) allowed us to reconstruct their morphology with little ambiguity. We found that all
251 VNC serotonergic neurons project quite locally, mostly within the same segment (**Fig. 5a**). Their
252 somas are located at a very ventral part of the VNC and their projections are mostly restricted
253 to the sensory zone (ventral half) of the VNC (**Fig. 5b**)[57,58].
254 As the majority of serotonergic neurons in the A2 to A8/9 segments of this VNC were labeled
255 and reconstructed, we paid extra attention to discover potential anatomical roles that respect
256 the repeated hemi-segment patterns of the VNC (**Fig. S13**). We noticed that all VNC
257 serotonergic neurons within the same hemi-segment send out co-fasciculated neurites that
258 form a single commissure projecting to the contralateral side (**S11e**, arrowheads). While
259 serotonergic neurons in the same hemi-segment have quite distinct morphologies and
260 projection patterns, they have similar counterparts in the contralateral hemi-segment,
261 therefore, forming a bi-lateral symmetric network (**Fig. 5c**, **5d**). These morphologically similar
262 neurons can be classified as at least 8 distinct subtypes based on the quantification of
263 morphological features, including projection density in the contralateral and the ipsilateral side,
264 major branching patterns and anterior *vs* posterior projection distribution (**Fig. 5d**, detailed in
265 **Methods**).

266 Discussion

267 We reported Bitbow, a set of novel transgenic tools capable of generating a large number of
268 unique imaging barcodes in a single animal (**Table 1**). Bitbow utilizes a novel design, in which
269 independent Flp/FRT recombination events lead to binary choices of expressing orthogonal
270 spectral labels. This mechanism exponentially expands the color-coding capacity to 2^N-1 when
271 using N "bits" of spectrally distinguishable tags. Targeting the same 5-FPs to 3 imaging
272 differentiable subcellular compartments, we created mngBitbow1.0 transgenic flies, which can
273 generate up to 32,767 unique Bitbow codes in a single brain. This is a significant advantage for
274 imaging-based lineage tracing studies because it greatly increases the possibility of labeling
275 neurons with unique lineage codes. Interestingly, we found that heat-shock induced
276 recombination events are constrained in neural stem cells of the larval Bitbow flies. Such
277 serendipity permits directly using Bitbow codes to determine lineage relationships between
278 neural progenies. Providing statistical quantification and modeling, we established that it is
279 feasible to map the lineage relationships between any subtype-specific neurons, driven by any
280 enhancer-Gal4, using fewer than ~10 brains.
281 In practice, we found that certain FP expressed with much higher frequencies than other
282 ones. We suspect that this is due to more frequently spinning of their flanking FRT sites under

suboptimal recombination conditions, such as heat-shock induced transient Flp activity. Bitbow codes containing these FPs would have higher collision rates when used in lineage mapping studies. We mitigate such disadvantage by excluding cells labeled by the high-frequency Bitbow codes from analysis. In the future, this problem can be avoided by screening more incompatible FRT sites and using only those with similar recombination efficiencies. Nonetheless, there are other disadvantages associated with heat-shock induced Flp recombination, especially for neuronal morphology labeling and reconstruction. As only the membrane Bitbow is suitable for morphology studies, we found a low percentage of cells were being labeled and their colors were relatively simple that neurons labeled by more than two FPs were relatively rare.

To solve the above-mentioned problems for morphology labeling and reconstruction, we generated Bitbow2 transgenic flies, in which a novel self-regulating Flp module was integrated to effectively recombine mBitbow1 without the need of heat-shock. The elimination of the *hs*-Flp allele yielded two additional advantages: 1) Needing only a simple cross to the broadly used Gal4 libraries, Bitbow2 can be used as a drop-in replacement to any UAS-FP reporters. 2) Abolishing the need for heat-shock, Bitbow2 is compatible with temperature-sensitive assays, such as heat-induced neuronal manipulations with shibire^{ts} [50], dTrpA1 [51], etc. Finally, we generated different versions of Bitbow2 flies, each of which labeled a different percentage of total neurons to suit the need of tuning the labeling density for different Gal4 driver lines.

Combining sample expansion (ExM) and saturated neuron tracing (nTracer), Bitbow2 flies are suitable for high-throughput morphology studies from light microscopy images. We found that Bitbow labeling is statistically consistent throughout the neuron soma and neurites. This builds the confidence of using fluorescence intensity difference in each spectral channel to differentiate neighboring neurons when using nTracer to reconstruct their morphology. We estimate that thousands (~5^5) of Bitbow “colors” can be easily distinguished in a well-taken 16-bit image dataset. Densely packed neurons, such as the VNC serotonergic neurons are now readily traceable to not only classify the morphological heterogeneity , but also reveal the neural network patterns among a genetically defined population. We envision that, in the future, combining with other high-throughput modalities, such as light-sheet microscopy and automated neuronal tracing, will make larger scale, multi-brain morphological studies feasible in most laboratories.

313 # Materials and Methods

314 ## Key Resources

315

REAGENT or RESOURCE	SOURCE	IDENTIFIER
Antibodies		
Rat Anti-mTFP	Cai Lab	
Chicken Anti-GFP	Cai Lab	
Rabbit Anti-mNeonGreen	Cai Lab	
Mouse Anti-mKusabira-Orange2	Cai Lab	
Guinea Pig Anti-mKate2	Cai Lab	
Alexa Fluor 594 Donkey Anti-Rat	Life Technologies	A21209
Alexa Fluor 488 Donkey Anti-Chicken	Jackson ImmunoResearch	703-545-155
Atto 490LS Goat Anti-Rabbit	Hypermol	2309
CF 555 Donkey Anti-Mouse	Sigma	SAB4600060
CF 633 Donkey Anti-Guinea Pig	Sigma	SAB4600129
Alexa Fluor 647 Donkey Anti-Guinea Pig	Jackson ImmunoResearch	706-605-148
Bacterial and Virus Strains		
Mach1-T1 Chemically Competent E. coli	Thermo Scientific	C862003
Stbl3 Chemically Competent E. coli	Thermo Scientific	C737303
Chemicals, Peptides, and Recombinant Proteins		
Acrylic acid N-hydroxysuccinimide ester	Sigma	A8060
Sodium Acrylate	Sigma	408220
Acrylamide	Sigma	A9099
N,N'-methylenebisacrylamide	Sigma	M7279
Tetramethylethylenediamine (TEMED)	Sigma	T7024
Ammonium Persulfate	Sigma	A3678
4-hydroxy-2,2,6,6-tetramethylpiperidin-1-oxyl (4HT)	Sigma	176141
Startingblock (PBS) blocking buffer	Thermo Scientific	37578
Proteinase K	NEB	P8107

Experimental Models: Cell Lines		
D. melanogaster: S2	Bing Ye Lab	
M. musculus: Neuro-2a	ATCC	CCL-131
Experimental Models: Organisms/Strains		
D. melanogaster: w1118;;	BDSC	RRID: BDSC_5905
D. melanogaster: hsFlp112;;	BDSC	
D. melanogaster: hsFlp112;Sp/CyO;TM2,Ubx/TM6B,Tb	Bing Ye Lab	
D. melanogaster: hsFlp112;;elav-Gal4	This study	
D. melanogaster: hsFlp112;TRH-Gal4;	This study	
D. melanogaster: yw;;mBitbow1.0	This study	
D. melanogaster: yw;;nBitbow1.0	This study	
D. melanogaster: yw;gBitbow1.0;	This study	
D. melanogaster: yw;gBitbow1.0/CyO;mBitbow1.0,nBitbow 1.0	This study	
D. melanogaster: yw;;mBitbow2.0	This study	
D. melanogaster: yw;;mBitbow2.1	This study	
D. melanogaster: yw;;2x[mBitbow2.0]	This study	
D. melanogaster: yw;;2x[mBitbow2.1]	This study	
D. melanogaster: w;elav-Gal4/CyO;	BDSC	8765
D. melanogaster: w;TRH-Gal4;	BDSC	38388
D. melanogaster: w;;R53C10-Gal4	BDSC	38873
D. melanogaster: w;;R67A06-Gal4	BDSC	39397
Recombinant DNA		
pmAmetrine-N1	Addgene	54505
pmTFP1-N1	Addgene	54521
pmNeonGreen-N1	Allele Biotechnology	
pmKusabira-Orange2-N1	[38]	
ptdKatushka2-N	[39]	
pmCitrine-N1	Addgene	54594
pmCherry-N1	[59]	
pJFRC-MUH	Addgene	26213

pattB-synaptobrevin-GAL4-hsp70	Addgene	46107
pJFRC81-10XUAS-IVS-Syn21-GFP-p10	Addgene	36432
pMT-Gal4	DGRC	1042
pUAST-Flp	DGRC	1020
pCAG-FlpINT	Dawen Cai Lab	
pDC-MUH	This study	
pDC-MUH-p10pA	This study	
pCMV-2xmAmetrine-N	This study	
pDC-UAS-mBitbow1.0	This study	
pDC-UAS-nBitbow1.0	This study	
pDC-UAS-gBitbow1.0	This study	
pDC-UAS-mBitbow2.0	This study	
pDC-UAS-mBitbow2.1	This study	
pAc5-Flp-p10pA	This study	
pCMV-3FRT-mCherry-F14-mTFP	This study	
pCMV-3FRT-mCherry-F15-mCit	This study	
pCMV-3FRT-F14-mTFP-F15-mCit	This study	
pCMV-3FRT-F14-F15-mCit-F13-mCherry	This study	
pCAG-Flpbow3	[10]	
Software and Algorithms		
Fiji	[60]	https://fiji.sc/
nTracer (Fiji plugin)	[31]	https://www.cai-lab.org/ntracer-tutorial
Spectral Unmixing (Fiji plugin)	Joachim Walter	https://imagej.nih.gov/ij/plugins/spectral-unmixing.html
Lasergene	DNASTAR	https://www.dnastar.com/
Graphpad Prism	Graphpad Software	https://www.graphpad.com/
Vaa3D	[61]	http://home.penglab.com/proj/vaa3d/home/
Blender	Blender Foundation	https://www.blender.org/
NumPy	NumPy.org	https://numpy.org/
umap-learn	[62]	https://github.com/lmcinnes/umap

316

317 ## *Drosophila* husbandry

318 Flies were reared at 25°C on standard CT medium with a 12h/12h light/dark cycle. For heat-
319 shock induced Bitbow labeling experiments, hsFlp;;elav-Gal4 or hsFlp;TRH-Gal4; females were
320 crossed to Bitbow1.0 males, and timed-egg-lay was conducted to collect embryos for the
321 desired time window in vials; afterwards, the vials were placed in a 37°C metal-bead bath for
322 30min to induce the heat-shock, and kept at 18°C to incubate until ready for dissection.

323 ## Molecular cloning and fly transgenics

324 To test out new incompatible FRT sites, a series of FRT-FP plasmids were constructed (**Fig.**
325 **S1**) using the mammalian expression backbone pCMV-N1 (Clontech). FRT-F13, FRT-F14 and FRT-
326 F15 sequences were obtained from a previous study [34], and introduced to the following
327 plasmids through PCRs. To test the incompatibility of FRT-F14 and FRT-F15 to three known FRTs
328 (FRT-F3, FRT-5T2, FRT-545), pCMV-3FRT-mCherry-F14-mTFP and pCMV-3FRT-mCherry-F15-mCit
329 were built through sequential assembly of the three FRTs from pCAG-Flybow (Cai lab), mCherry-
330 SV40pA from pmCherry-N1 (Addgene), and F14-mTFP-SV40pA or F15-mCitrine-SV40pA from
331 pmTFP-N1 or pmCit-N1 (Addgene), respectively, using PCR, restriction digestion, and ligation.
332 After the incompatibility test was done, mCherry-pA was removed by digestion with two
333 flanking blunt-end sites (PmlI, EcoRV), and re-ligation to produce pCMV-3FRT-F14-mTFP and
334 pCMV-3FRT-F15-mCit, as the control plasmids. Similar cloning approaches were applied in the
335 next steps. To test incompatibility of FRT-F15 to the other four FRT sites, F15-mCit-pA was
336 moved into pCMV-3FRT-F14-mTFP to produce pCMV-3FRT-F14-mTFP-F15-mCit, from which
337 mTFP-SV40pA was removed to produce the control plasmid pCMV-3FRT-F14-F15-mCit. Finally,
338 to test incompatibility of FRT-F13 to the other five FRT sites, F13-mCherry-pA was moved into
339 pCMV-3FRT-F14-F15-mCit to produce pCMV-3FRT-F14-F15-mCit-F13-mCherry, from which
340 mCitrine-SV40pA was removed to produce the control plasmid pCMV-3FRT-F14-F15-F13-
341 mCherry.

342 For Bitbow1 plasmids, cDNAs encoding the following FPs were used: mAmetrine, mTFP,
343 mNeonGreen, mKusabira-Orange2, and tdKatushka2 [35–39]. *Drosophila* myristoylation signal
344 peptide of dSrc64B (1-10aa, dMyr), Human histone 2B protein (full length, hH2B) or Mouse
345 Mannosidase II alpha 1 (1-112aa, mManII) was fused in-frame to the N-terminus of individual
346 FPs (dMyr-FP, hH2B-FP, mMannII-FP), to achieve targeted labeling at the cell membrane,
347 nucleus or Golgi apparatus [63–65]. Individual incompatible FRT sequence pairs (FRT-F13, FRT-F14,
348 FRT-545, FRT-F3, or FRT-5T2) [10,34,66–68] were then placed in the opposing direction to flank
349 dMyr-FP / hH2B-FP / mMannII-FP sequence. An upstream activation sequence (UAS) and a p10
350 polyadenylation sequence (p10pA) [69] were placed upstream and downstream of each FRT
351 flanked FP cassettes, respectively, and separately cloned into pDC-MUH, which was based on
352 the pJFRC-MUH backbone vector[70] with a few digestion site modifications, by standard cloning

353 methods. The Bitbow1.0 plasmids were finally assembled together from the five individual
354 modules through Gibson assembly [71].
355 For Bitbow2 plasmids, the nSyb-promoter-driving self-regulating flippase module was
356 constructed by flanking FlpINT (flippase with an inserted c. elegans intron [72], Cai lab) cDNA with
357 a FRT-F14 pair or a FRT-F15 pair which were oriented in the same direction, and then placed
358 downstream of a *Drosophila* n-Synaptobrevin promoter [73]. The module was then inserted into
359 the mBitbow1.0 plasmid, at a location far away from all 5 FP modules, through Gibson
360 Assembly to generate mBitbow2.0 or mBitbow2.1.
361 The final Bitbow plasmids were integrated into *Drosophila melanogaster* genome docking
362 sites attP40, attP2 or VK00027 (**Table 1**) through ΦC31-integrase-mediated transgenesis [74–78].
363 Embryo injections and transgenic selections were done by BestGene Inc (Chino Hills, CA).

364 ## Dissection and mounting

365 Adult or 3rd instar *Drosophila* brains were dissected in PBS at room temperature (abbr. RT)
366 within 30min before proceeding to fixation. Dissected brains were fixed in 4% PFA (Sigma
367 #P6148, diluted in PBS) at RT with gentle nutation for 20min, followed by three quick PBST
368 (PBS+1% Triton X-100) washes, then PBS washes for 15min x 3. Brains then either proceeded to
369 direct mounting (for native fluorescence imaging) or immuno-stainings. Vectashield (Vector
370 Laboratories, H-1000) was used as the mounting medium.

371 ## Immunohistochemistry

372 Fixed brain samples were treated with StartingBlock (Thermo, 37578) for 1 hour at RT with
373 gentle nutation. After blocking, the brains were incubated with primary antibodies diluted in
374 StartingBlock for 2 overnights at 4°C. Three quick PBST washes and PBS washes for 15min x 3
375 were done, before the brains were incubated with secondary antibodies diluted in
376 StartingBlock for 2 overnights at 4°C. Finally three quick PBST washes and PBS washes for 15min
377 x 3 were done and the brains were ready for imaging. For detailed antibody combinations and
378 dilutions see ***Key-resource-table***.

379 ## Expansion Microscopy (ExM)

380 ExM brain samples were generated following the ProExM protocol [54] with modifications.
381 Antibody-stained Bitbow samples were treated in Acrylic acid N-hydroxysuccinimide ester (AaX,
382 Sigma, A8060) at RT for 1 overnight, followed by PBS washes for 15min x 3. Samples were then
383 incubated in the ExM monomer solution ("Stock-X", containing Acrylate, Acrylamide, and Bis-
384 acrylamide) at 4°C for 1 overnight. Samples were transferred to fresh ExM monomer solution
385 with gel initiators (APS, TEMED, 4-HT) at 4°C for 15min, and then quickly mounted on a sample
386 chamber made with 200µm adaptors (Sun lab) on a glass slide, sealed with a 22x30 coverslip on
387 top (Fisher, 12-544). The slide was then transferred to a humidity box and incubated at 37°C for
388 about 2 hours until the gel fully polymerized. The gel was trimmed carefully with a razor to
389 allow as little of excessive space around the brains as possible. Trimmed gel pieces were

390 transferred to an EP tube and digested with Proteinase K (NEB, P8107) at 37°C for 1 hour. Three
391 quick PBST washes and PBS washes for 15min x 3 were done before the brains were put into
392 another round of antibody staining, following the same IHC protocol mentioned above. After
393 the second-round staining, the gels were slowly expanded to the final size by changing the
394 submerging solution from PBS to pure diH2O, and ready for imaging.

395 ## Confocal microscopy and linear unmixing

396 Confocal images were acquired with Zeiss LSM780 with a 20x 1.0 NA water immersion
397 objective (421452-9800-000) or a 40x 1.3 NA oil immersion objective (421762-9900-000). The
398 32-channel GaAsP array detector was used to allow multi-track detection of five fluorophores
399 with proper channel collection setups (**Fig. S2**).

400 Spectral Unmixing plug-in (by Joachim Walter) in Fiji was used to perform linear unmixing on
401 Bitbow images. Reference unmixing matrix was measured by imaging cultured mouse N2A cells
402 expressing mAmetrine, mTFP, mNeonGreen, mKO2 or tdKatushka2 separately, with the exact
403 same multi-track setups intended for Bitbow brains. Customized ImageJ scripts were used to
404 automate the unmixing process as well as creating composite image stacks from unmixed
405 channels.

406 ## Image stitching and neuron tracing

407 When the region of interest was larger than the objective field of view, multiple confocal
408 tiles were taken and stitched offline. 5% overlapping seams were set between adjacent tiles to
409 allow reliable stitching and maximize the area of coverage. Alignmaster 1.0.6 (part of the
410 nTracer tool set) was used to perform stitching between tiles sequentially.

411 All neuronal tracings were done using nTracer 1.3.5 [31]. Sampling tolerance for color and
412 intensity were set at 0.3 to allow accurate and efficient tracings. Tracing results were exported
413 in SWC format for downstream 3D-rendering and Bitbow color analysis.

414 3D visualizations of neuron tracings were performed using custom scripts in the open-source
415 modeling software Blender v2.81 (Blender Foundation). Models containing fluorescence data
416 were produced with a modification of the method described in [79].

417 ## Quantification and statistical analysis

418 *Bitbow code quantifications*

419 Bitbow-labeled neural clusters in the 3rd instar larval brains were used to quantify the
420 labeling performance of 1-localization, 2-localization, and 3-localization Bitbows. Clusters in the
421 central brain, gnathal segments, and thoracic segments were marked with the Fiji ROI tool, and
422 the on/off status of each color channel in every cluster was manually recorded as 1/0 for each
423 "bit" (examples in **Fig. 1e, 2f**). The frequency of occurrence of each Bitbow module was
424 calculated in each brain, and summarized across multiple brains with the mean and standard
425 deviation of the frequency reported (**Fig. 1h, S7a**). 15-module frequencies of mngBitbow were

used to generate empirical probability distribution of all 32,767 mngBitbow codes, which was further used in simulations described in **Fig. 2g, 2j** (details below).

Bitbow color differentiation and stability analysis

Pixel intensity values from 5 channels along the tracing of all 21 somas and part of 4 neurites (A5L1, A5L2, A5R1, A5R2) were used to generate analysis on differentiation power as well as the stability of Bibtow labeling. Raw intensities were processed through a 3x3x3 median kernel and a 10-pixel rolling window average to reduce noise, then the pixel intensity in each channel was normalized to the sum of five channels of that pixel, in order to bring brighter and dimmer pixels to the same scale for accurate color analysis.

To visualize the differentiation power using all five Bitbow channels, UMAP was used on the 21 somas to reduce the five-dimension pixel values onto a 2D embedding. To visualize differences between 4 relatively closely-located neurons on the 21-soma embedding, an independent UMAP was generated with only those 4 neurons using the same parameters. Data were processed with Python 3.7.4 and umap-learn 0.3.10.

To visualize the stability of Bitbow labeling, soma pixel intensities and neurite pixel intensities from the same neurons were summarized in “split-violin” plots, where in each plot the left half represents soma pixels and the right half neurite pixels.

Simulations of Bitbow labeling requirements

Computer simulations were used to estimate the number of animals required to achieve saturated coverage for a range of hypothetical N-neuron systems (**Fig. 2j**). For each condition, 500 trials of Algorithm 1 were averaged using custom code implemented in Python v3.7.4 and NumPy v1.17.2. Here, *activation_rate* was assigned to estimates of 0.5% (MARCM) and 48.08% (Bitbow) to model differences in labeling densities. The whitelist array *valid_barcodes* was assigned as the k lowest-probability barcodes (32,767, 32,700 or 32,000) for the Bitbow trials or all possible barcodes for MARCM.

Algorithm 1:

```
def monte_carlo_trial( cell_count, activation_rate  ):
      counter ← 0
      cell_hist ← [ 0 ] * cell_count

      while minimum( cell_hist ) <  1 do
            cell_array ← [ NULL ] * cell_count
            for i ← 0 to cell_count do
                let x be a random variate from the respective
                barcode distribution
```

```
                if rand(0, 1) > activation_rate then
                    x ← NULL
                else if x not in valid_barcodes then
                    x ← NULL
                cell_array(i) ← x

                for i ← 0 to cell_count do
                    if cell_array(i) not unique in cell_array do
                        cell_array(i) ← NULL
                for i ← 0 to cell_count do
                    if cell_array(i) ≠ NULL then
                        cell_hist(i) ← cell_hist(i) + 1
                counter ← counter + 1
        yield counter
```

Simulations of Bitbow barcode collision rate

Simulations of the empirical collision rate (**Fig. 2g**) were performed in a similar manner. Briefly, random lists of barcodes were drawn from the empirical distributions, followed by the counting of repeated barcodes to produce an overlap rate. This process was repeated 100,000 times for systems under 100 lineages, 1,000 times for systems between 100 and 1000 lineages, and 10 times between 1,000 and 1,000,000 lineages, due to computational complexity.

Data Availability

The data that support the findings of this study are available from the corresponding author upon reasonable request.

Code Availability

Custom code for analysis of image processing and data analysis is available from the corresponding author upon reasonable request.

Acknowledgments

We thank all members of the Cai lab who contribute to the discussion and revision of the manuscript. We thank Bing Ye for providing several transgenic *Drosophila* lines. We thank Grace Hyunh and Ed Boyden for their advice on expansion microscopy. YL acknowledges support by the Patten Fellowship. MG acknowledges support by the University of Michigan UROP summer fellowship. DC acknowledges support by NIH 1R01AI130303, 1UF1NS107659, 1R01MH110932, and 1RF1MH120005, and by National Science Foundation NeuroNex-1707316.

Author Contributions

DC conceived and supervised the project. YL and DC designed the experiments. YL, LAW and DC wrote the manuscript with input from all authors. YL designed cloning strategies to construct Bitbow plasmids. YL, YZ, MG, TYC and DHR generated the Bitbow transgenic flies. YL, YZ, and EME processed brain samples and performed microscopy. YL and MC quantified the Bitbow1 lineage codes. YL and EME quantified Bitbow2 labeling coverage. YL and HPJC traced the VNC serotonergic neurons. LAW, YL, NSM and DC established the statistical models. YL wrote the codes for Bitbow color analysis. LAW wrote the codes for simulations and scripts for 3D renderings of traced neurons.

References

1. Ramon y Cajal, S. Histologie du système nerveux de l'homme et des vertébrés. *Maloine Paris* **2**, 153–173 (1911).
2. Golgi, C. *Sulla fina anatomia degli organi centrali del sistema nervoso*. (S. Calderini, 1885).
3. Lee, T. & Luo, L. Mosaic analysis with a repressible cell marker for studies of gene function in neuronal morphogenesis. *Neuron* **22**, 451–461 (1999).
4. Muzumdar, M. D., Luo, L. & Zong, H. Modeling sporadic loss of heterozygosity in mice by using mosaic analysis with double markers (MADM). *Proc Natl Acad Sci U A* **104**, 4495–4500 (2007).
5. Livet, J. *et al.* Transgenic strategies for combinatorial expression of fluorescent proteins in the nervous system. *Nature* **450**, 56–62 (2007).
6. Lichtman, J. W., Livet, J. & Sanes, J. R. A technicolour approach to the connectome. *Nat. Rev. Neurosci.* **9**, 417–422 (2008).
7. Richier, B. & Salecker, I. Versatile genetic paintbrushes: Brainbow technologies. *WIREs Dev. Biol.* **4**, 161–180 (2015).
8. Weissman, T. A. & Pan, Y. A. Brainbow: new resources and emerging biological applications for multicolor genetic labeling and analysis. *Genetics* **199**, 293–306 (2015).
9. Snippert, H. J. *et al.* Intestinal Crypt Homeostasis Results from Neutral Competition between Symmetrically Dividing Lgr5 Stem Cells. *Cell* **143**, 134–144 (2010).
10. Cai, D., Cohen, K. B., Luo, T., Lichtman, J. W. & Sanes, J. R. Improved tools for the Brainbow toolbox. *Nat Methods* **10**, 540–547 (2013).
11. Hampel, S. *et al.* Drosophila Brainbow: a recombinase-based fluorescence labeling technique to subdivide neural expression patterns. *Nat Methods* **8**, 253–259 (2011).
12. Hadjieconomou, D. *et al.* Flybow: genetic multicolor cell labeling for neural circuit analysis in Drosophila melanogaster. *Nat. Methods* **8**, 260–266 (2011).
13. Förster, D. & Luschnig, S. Src42A-dependent polarized cell shape changes mediate epithelial tube elongation in Drosophila. *Nat. Cell Biol.* **14**, 526–534 (2012).

534 14. Boulina, M., Samarajeewa, H., Baker, J. D., Kim, M. D. & Chiba, A. Live imaging of multicolor-
535 labeled cells in Drosophila. *Development* **140**, 1605–1613 (2013).
536 15. Worley, M. I., Setiawan, L. & Hariharan, I. K. TIE-DYE: a combinatorial marking system to
537 visualize and genetically manipulate clones during development in Drosophila
538 melanogaster. *Development* **140**, 3275–3284 (2013).
539 16. Kanca, O., Caussinus, E., Denes, A. S., Percival-Smith, A. & Affolter, M. Raeppli: a whole-
540 tissue labeling tool for live imaging of Drosophila development. *Development* **141**, 472–480
541 (2014).
542 17. Chin, A.-L., Lin, C.-Y., Fu, T.-F., Dickson, B. J. & Chiang, A.-S. Diversity and wiring variability of
543 visual local neurons in the Drosophila medulla M6 stratum. *J. Comp. Neurol.* **522**, 3795–
544 3816 (2014).
545 18. Pan, Y. A., Livet, J., Sanes, J. R., Lichtman, J. W. & Schier, A. F. Multicolor Brainbow Imaging
546 in Zebrafish. *Cold Spring Harb. Protoc.* **2011**, pdb.prot5546 (2011).
547 19. Gupta, V. & Poss, K. D. Clonally dominant cardiomyocytes direct heart morphogenesis.
548 *Nature* **484**, 479–484 (2012).
549 20. Pan, Y. A. *et al.* Zebrabow: multispectral cell labeling for cell tracing and lineage analysis in
550 zebrafish. *Development* **140**, 2835–2846 (2013).
551 21. Robles, E., Filosa, A. & Baier, H. Precise Lamination of Retinal Axons Generates Multiple
552 Parallel Input Pathways in the Tectum. *J. Neurosci.* **33**, 5027 (2013).
553 22. Barbier, M. & Damron, F. H. Rainbow Vectors for Broad-Range Bacterial Fluorescence
554 Labeling. *PLOS ONE* **11**, e0146827 (2016).
555 23. Kobiler, O., Lipman, Y., Therkelsen, K., Daubechies, I. & Enquist, L. W. Herpesviruses carrying
556 a Brainbow cassette reveal replication and expression of limited numbers of incoming
557 genomes. *Nat. Commun.* **1**, 1–8 (2010).
558 24. Chan, K. Y. *et al.* Engineered AAVs for efficient noninvasive gene delivery to the central and
559 peripheral nervous systems. *Nat Neurosci* **20**, 1172–1179 (2017).
560 25. Sakaguchi, R., Leiwe, M. N. & Imai, T. Bright multicolor labeling of neuronal circuits with
561 fluorescent proteins and chemical tags. *eLife* **7**, e40350 (2018).
562 26. Loulier, K. *et al.* Multiplex cell and lineage tracking with combinatorial labels. *Neuron* **81**,
563 505–520 (2014).
564 27. García-Moreno, F., Vasistha, N. A., Begbie, J. & Molnár, Z. CLoNe is a new method to target
565 single progenitors and study their progeny in mouse and chick. *Development* **141**, 1589–
566 1598 (2014).
567 28. Nern, A., Pfeiffer, B. D. & Rubin, G. M. Optimized tools for multicolor stochastic labeling
568 reveal diverse stereotyped cell arrangements in the fly visual system. *Proc Natl Acad Sci U A*
569 **112**, E2967-76 (2015).
570 29. Hammer, S., Monavarfeshani, A., Lemon, T., Su, J. & Fox, M. A. Multiple Retinal Axons

571 Converge onto Relay Cells in the Adult Mouse Thalamus. *Cell Rep* **12**, 1575–1583 (2015).
572 30. Takesian, A. E., Bogart, L. J., Lichtman, J. W. & Hensch, T. K. Inhibitory circuit gating of
573 auditory critical-period plasticity. *Nat Neurosci* **21**, 218–227 (2018).
574 31. Roossien, D. H. *et al.* Multispectral tracing in densely labeled mouse brain with nTracer.
575 *Bioinformatics* **35**, 3544–3546 (2019).
576 32. Shen, F. Y. *et al.* Light microscopy based approach for mapping connectivity with molecular
577 specificity. *bioRxiv* 2020.02.24.963538 (2020) doi:10.1101/2020.02.24.963538.
578 33. Veling, M. W. *et al.* Identification of Neuronal Lineages in the Drosophila Peripheral
579 Nervous System with a "Digital" Multi-spectral Lineage Tracing System. *Cell Rep.* **29**, 3303-
580 3312.e3 (2019).
581 34. Turan, S., Kuehle, J., Schambach, A., Baum, C. & Bode, J. Multiplexing RMCE: versatile
582 extensions of the Flp-recombinase-mediated cassette-exchange technology. *J Mol Biol* **402**,
583 52–69 (2010).
584 35. Ai, H.-W., Henderson, J. N., Remington, S. J. & Campbell, R. E. Directed evolution of a
585 monomeric, bright and photostable version of Clavularia cyan fluorescent protein:
586 structural characterization and applications in fluorescence imaging. *Biochem J* **400**, 531–
587 540 (2006).
588 36. Ai, H.-W., Hazelwood, K. L., Davidson, M. W. & Campbell, R. E. Fluorescent protein FRET
589 pairs for ratiometric imaging of dual biosensors. *Nat Methods* **5**, 401–403 (2008).
590 37. Shaner, N. C. *et al.* A bright monomeric green fluorescent protein derived from
591 Branchiostoma lanceolatum. *Nat Methods* **10**, 407–409 (2013).
592 38. Sakaue-Sawano, A. *et al.* Visualizing spatiotemporal dynamics of multicellular cell-cycle
593 progression. *Cell* **132**, 487–498 (2008).
594 39. Shcherbo, D. *et al.* Far-red fluorescent tags for protein imaging in living tissues. *Biochem J*
595 **418**, 567–574 (2009).
596 40. Yu, H.-H. *et al.* A Complete Developmental Sequence of a Drosophila Neuronal Lineage as
597 Revealed by Twin-Spot MARCM. *PLoS Biol.* **8**, e1000461 (2010).
598 41. Yu, H.-H. *et al.* Clonal Development and Organization of the Adult Drosophila Central Brain.
599 *Curr. Biol.* **23**, 633–643 (2013).
600 42. Lacin, H., Zhu, Y., Wilson, B. A. & Skeath, J. B. Transcription factor expression uniquely
601 identifies most postembryonic neuronal lineages in the Drosophila thoracic central nervous
602 system. *Development* **141**, 1011–1021 (2014).
603 43. Yuan, Q., Joiner, W. J. & Sehgal, A. A sleep-promoting role for the Drosophila serotonin
604 receptor 1A. *Curr Biol* **16**, 1051–1062 (2006).
605 44. Sitaraman, D. *et al.* Serotonin is necessary for place memory in Drosophila. *Proc Natl Acad*
606 *Sci U A* **105**, 5579–5584 (2008).
607 45. Becnel, J., Johnson, O., Luo, J., Nässel, D. R. & Nichols, C. D. The serotonin 5-HT7Dro

608 receptor is expressed in the brain of Drosophila, and is essential for normal courtship and
609 mating. *PLoS One* **6**, e20800 (2011).
610 46. Johnson, O., Becnel, J. & Nichols, C. D. Serotonin receptor activity is necessary for olfactory
611 learning and memory in Drosophila melanogaster. *Neuroscience* **192**, 372–381 (2011).
612 47. Liu, Y. *et al.* Molecular regulation of sexual preference revealed by genetic studies of 5-HT in
613 the brains of male mice. *Nature* **472**, 95–99 (2011).
614 48. Gasque, G., Conway, S., Huang, J., Rao, Y. & Vosshall, L. B. Small molecule drug screening in
615 Drosophila identifies the 5HT2A receptor as a feeding modulation target. *Sci Rep* **3**,
616 srep02120 (2013).
617 49. Vallés, A. M. & White, K. Serotonin-containing neurons in Drosophila melanogaster:
618 development and distribution. *J Comp Neurol* **268**, 414–428 (1988).
619 50. Kitamoto, T. Conditional modification of behavior in Drosophila by targeted expression of a
620 temperature-sensitive shibire allele in defined neurons. *J Neurobiol* **47**, 81–92 (2001).
621 51. Hamada, F. N. *et al.* An internal thermal sensor controlling temperature preference in
622 Drosophila. *Nature* **454**, 217–220 (2008).
623 52. Riabinina, O. *et al.* Improved and expanded Q-system reagents for genetic manipulations.
624 *Nat Methods* **12**, 219–22, 5 p following 222 (2015).
625 53. Peng, H. *et al.* BrainAligner: 3D registration atlases of Drosophila brains. *Nat Methods* **8**,
626 493–500 (2011).
627 54. Tillberg, P. W. *et al.* Protein-retention expansion microscopy of cells and tissues labeled
628 using standard fluorescent proteins and antibodies. *Nat Biotechnol* **34**, 987–992 (2016).
629 55. Cahoon, C. K. *et al.* Superresolution expansion microscopy reveals the three-dimensional
630 organization of the synaptonemal complex. *Proc Natl Acad Sci U A* **114**, E6857–E6866
631 (2017).
632 56. Gao, R. *et al.* Cortical column and whole-brain imaging with molecular contrast and
633 nanoscale resolution. *Science* **363**, (2019).
634 57. Sykes, P. A. & Condron, B. G. Development and sensitivity to serotonin of Drosophila
635 serotonergic varicosities in the central nervous system. *Dev. Biol.* **286**, 207–216 (2005).
636 58. Chen, J. & Condron, B. G. Branch architecture of the fly larval abdominal serotonergic
637 neurons. *Dev. Biol.* **320**, 30–38 (2008).
638 59. Shaner, N. C. *et al.* Improved monomeric red, orange and yellow fluorescent proteins
639 derived from Discosoma sp. red fluorescent protein. *Nat. Biotechnol.* **22**, 1567–1572 (2004).
640 60. Schindelin, J. *et al.* Fiji: an open-source platform for biological-image analysis. *Nat. Methods*
641 **9**, 676–682 (2012).
642 61. Peng, H., Ruan, Z., Long, F., Simpson, J. H. & Myers, E. W. V3D enables real-time 3D
643 visualization and quantitative analysis of large-scale biological image data sets. *Nat.*
644 *Biotechnol.* **28**, 348–353 (2010).

645 62. McInnes, L., Healy, J. & Melville, J. UMAP: Uniform Manifold Approximation and Projection
646 for Dimension Reduction. *ArXiv180203426 Cs Stat* (2018).
647 63. Kanda, T., Sullivan, K. F. & Wahl, G. M. Histone–GFP fusion protein enables sensitive
648 analysis of chromosome dynamics in living mammalian cells. *Curr. Biol.* **8**, 377–385 (1998).
649 64. Struhl, G. & Adachi, A. Nuclear Access and Action of Notch In Vivo. *Cell* **93**, 649–660 (1998).
650 65. Ye, B. *et al.* Growing Dendrites and Axons Differ in Their Reliance on the Secretory Pathway.
651 *Cell* **130**, 717–729 (2007).
652 66. McLeod, M., Craft, S. & Broach, J. R. Identification of the crossover site during FLP-mediated
653 recombination in the Saccharomyces cerevisiae plasmid 2 microns circle. *Mol. Cell. Biol.* **6**,
654 3357–3367 (1986).
655 67. Schlake, T. & Bode, J. Use of Mutated FLP Recognition Target (FRT) Sites for the Exchange of
656 Expression Cassettes at Defined Chromosomal Loci. *Biochemistry* **33**, 12746–12751 (1994).
657 68. Volkert, F. C. & Broach, J. R. Site-specific recombination promotes plasmid amplification in
658 yeast. *Cell* **46**, 541–550 (1986).
659 69. Pfeiffer, B. D., Truman, J. W. & Rubin, G. M. Using translational enhancers to increase
660 transgene expression in Drosophila. *Proc. Natl. Acad. Sci.* **109**, 6626–6631 (2012).
661 70. Pfeiffer, B. D. *et al.* Refinement of Tools for Targeted Gene Expression in Drosophila.
662 *Genetics* **186**, 735–755 (2010).
663 71. Gibson, D. G. *et al.* Enzymatic assembly of DNA molecules up to several hundred kilobases.
664 *Nat. Methods* **6**, 343–345 (2009).
665 72. Davis, M. W., Morton, J. J., Carroll, D. & Jorgensen, E. M. Gene Activation Using FLP
666 Recombinase in C. elegans. *PLoS Genet.* **4**, e1000028 (2008).
667 73. Riabinina, O. *et al.* Improved and expanded Q-system reagents for genetic manipulations.
668 *Nat. Methods* **12**, 219–222 (2015).
669 74. Bateman, J. R., Lee, A. M. & Wu, C. -ting. Site-Specific Transformation of Drosophila via
670 φC31 Integrase-Mediated Cassette Exchange. *Genetics* **173**, 769–777 (2006).
671 75. Bischof, J., Maeda, R. K., Hediger, M., Karch, F. & Basler, K. An optimized transgenesis
672 system for Drosophila using germ-line-specific C31 integrases. *Proc. Natl. Acad. Sci.* **104**,
673 3312–3317 (2007).
674 76. Groth, A. C. Construction of Transgenic Drosophila by Using the Site-Specific Integrase From
675 Phage C31. *Genetics* **166**, 1775–1782 (2004).
676 77. Markstein, M., Pitsouli, C., Villalta, C., Celniker, S. E. & Perrimon, N. Exploiting position
677 effects and the gypsy retrovirus insulator to engineer precisely expressed transgenes. *Nat.
678 Genet.* **40**, 476–483 (2008).
679 78. Venken, K. J. T., He, Y., Hoskins, R. A. & Bellen, H. J. P[acman]: A BAC Transgenic Platform
680 for Targeted Insertion of Large DNA Fragments in D. melanogaster. *Science* **314**, 1747–1751
681 (2006).

682 79. Haschka, T., Dauchez, M. & Henon, E. Visualization of molecular properties at the qantum
683 mechanical level using blender. in *2015 IEEE 1st International Workshop on Virtual and*
684 *Augmented Reality for Molecular Science (VARMS@IEEEVR)* 7–13 (IEEE, 2015).
685 doi:10.1109/VARMS.2015.7151719.

686

Table 1. Transgenic *Drosophila* Bitbow summary.

Bitbow version	Subcellular compartment	Insertion site (Chr.)	self-regulating Flp	Labeling density
mBitbow 1.0	Cell membrane	attP40(2L) or attP2(3L)	No	Variable (with hsFlp)
nBitbow 1.0	Nucleus	attP40(2L) or VK27(3R)	No	Variable (with hsFlp)
gBitbow 1.0	Golgi	attP40(2L) or attP2(3L)	No	Variable (with hsFlp)
mBitbow 2.0	Cell membrane	attP2(3L) or VK27(3R)	Yes	Medium (40%-60%)
mBitbow 2.1	Cell membrane	attP2(3L) or VK27(3R)	Yes	High (70%-95%)

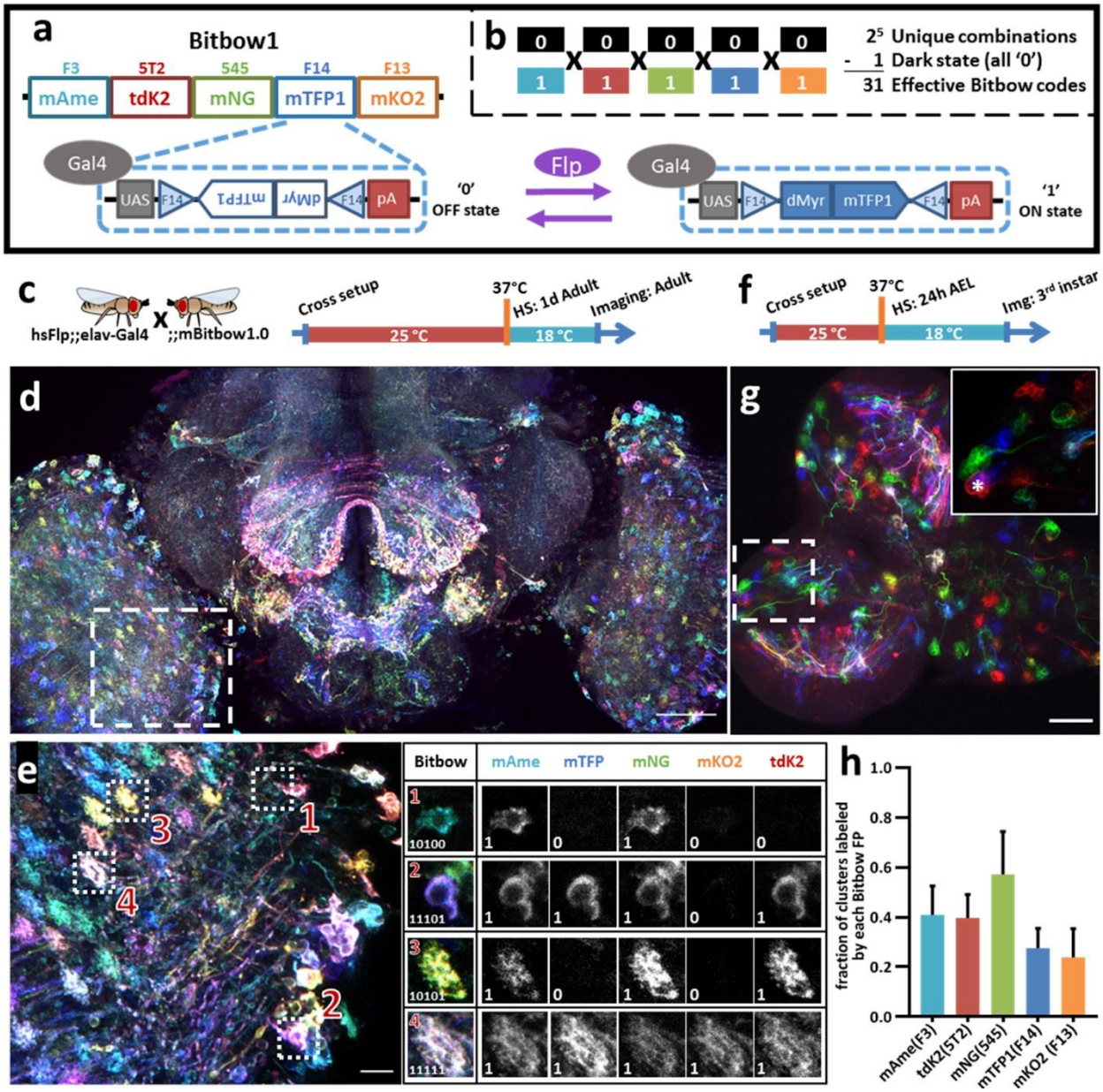
a
Bitbow1
F3
5T2
545
F14
F13
mAme
tdK2
mNG
mTFP1
mKO2
Gal4
UAS
F14
mTFP1
dMyr
F14
pA
'0'
OFF state
Flp
Gal4
UAS
F14
dMyr
mTFP1
F14
pA
'1'
ON state
b
0
1
2⁵ Unique combinations
- 1 Dark state (all '0')
31 Effective Bitbow codes
c
hsFlp;;elav-Gal4
;;mBitbow1.0
Cross setup
37°C
HS: 1d Adult
Imaging: Adult
25 °C
18 °C
f
Cross setup
37°C
HS: 24h AEL
Img: 3rd instar
25 °C
18 °C
d
g
e
1
2
3
4
Bitbow
mAme
mTFP
mNG
mKO2
tdK2
10100
11101
10101
11111
h
fraction of clusters labeled by each Bitbow FP
1.0
0.8
0.6
0.4
0.2
0.0
mAme(F3)
tdK2(5T2)
mNG(545)
mTFP1(F14)
mKO2 (F13)

Figure 1. Bitbow1 design and characterization of labeling properties. (a) Schematic of Bitbow1 design. Five spectrally distinct fluorescent proteins (FPs) are separated by five pairs of reversely positioned orthogonal FRT sites. The mTFP/FRT-F14 module is shown in the dashed box. The FP's open reading frame (ORF) is positioned in the reverse direction, corresponding to an default OFF state ('0'). Upon Flp induced recombination, the FP's ORF may spin to the forward direction for Gal4 driven expression, corresponding to an ON state ('1'). **(b)** 31 Bitbow color codes could be generated in a single Bitbow1 brain. **(c)** A hsFlp;;elav-Gal4 driver fly was crossed to the mBitbow1.0 fly to examine the offspring expression in the nervous system upon heat-shock induced Flp activity. Experimental setups of adult heat shock-induced labeling. **(d)** Maximum intensity projection overview of an adult heat-chocked brain. **(e)** Left panel, enlarged boxed region in (**d**) showed individual neurons are labeled in distinct colors, i.e., Bitbow codes. Right panel, Bitbow codes of four selected optic lobe neurons' somas or terminals. **(f)** Experimental setups of generating heat shock-induced Bitbow labeling in 3rd instar brains. **(g)** Maximum intensity projection overview of a 3rd instar larvae heat-chocked brain. Inset, the enlarged boxed region showed clusters of cells labeled in the same colors. Asterisk indicates a neuroblast. **(h)** Quantification of occurrence frequencies of each Bitbow color. Among all quantified clusters, the fraction of clusters containing each Bitbow color were displayed. 787 clusters from 6 brains are included. Error bars are SD. HS, heat-shock. Img, imaging. Scale bars: (**d**, **g**) 50µm, (**e**) 10µm.

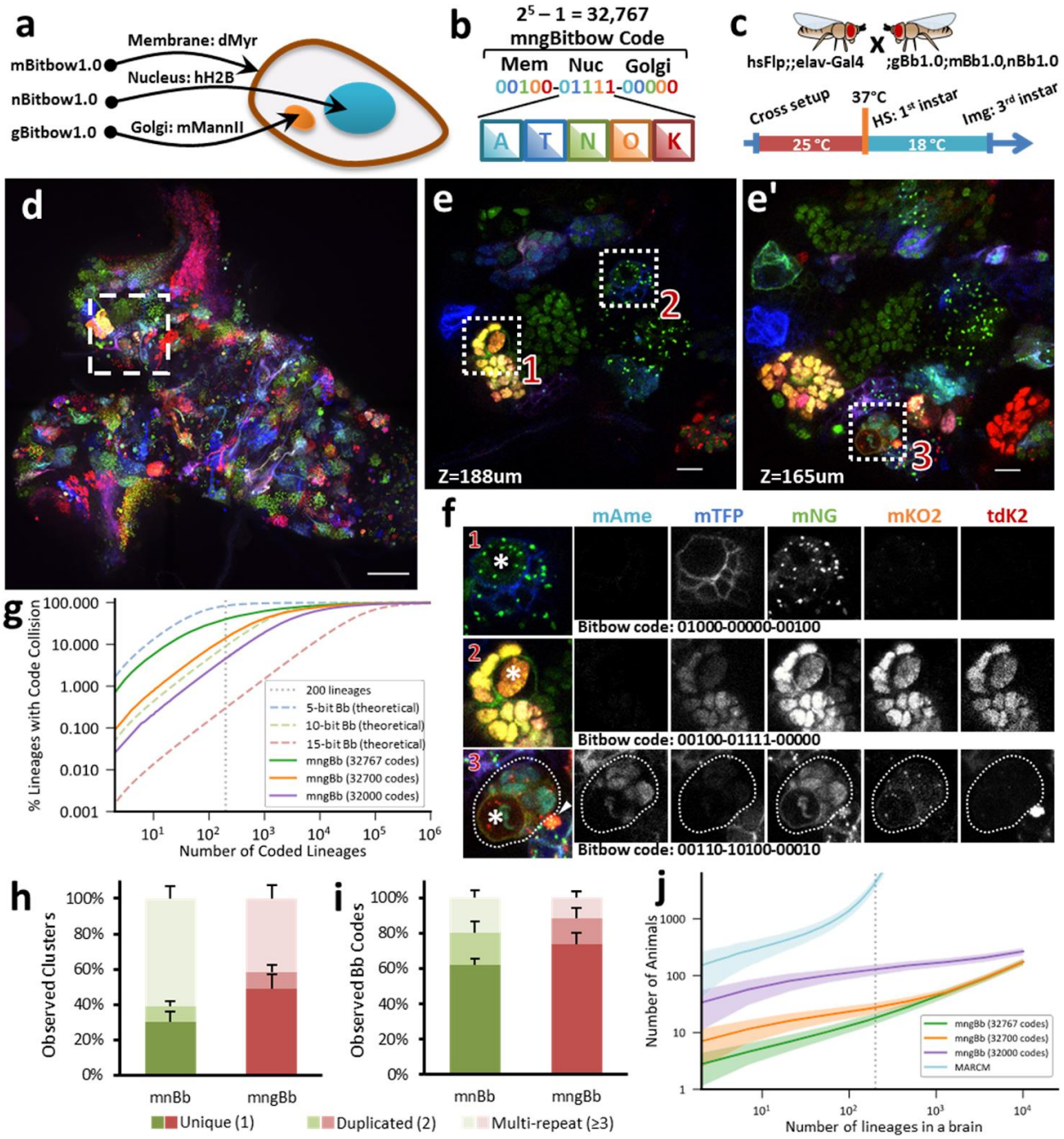
a
Membrane: dMyr
mBitbow1.0
Nucleus: hH2B
nBitbow1.0
Golgi: mMannII
gBitbow1.0
b
2^5 – 1 = 32,767
mngBitbow Code
Mem Nuc Golgi
00100-01111-00000
A T N O K
c
hsFlp;;elav-Gal4
x
;gBb1.0;mBb1.0,nBb1.0
Cross setup
37°C
HS: 1st instar
Img: 3rd instar
25 °C
18 °C
d
e
e'
Z=188um
Z=165um
f
mAme
mTFP
mNG
mKO2
tdK2
Bitbow code: 01000-00000-00100
Bitbow code: 00100-01111-00000
Bitbow code: 00110-10100-00010
g
% Lineages with Code Collision
Number of Coded Lineages
200 lineages
5-bit Bb (theoretical)
10-bit Bb (theoretical)
15-bit Bb (theoretical)
mngBb (32767 codes)
mngBb (32700 codes)
mngBb (32000 codes)
h
Observed Clusters
mnBb
mngBb
i
Observed Bb Codes
mnBb
mngBb
Unique (1)
Duplicated (2)
Multi-repeat (≥3)
j
Number of Animals
Number of lineages in a brain
mngBb (32767 codes)
mngBb (32700 codes)
mngBb (32000 codes)
MARCM

708

Figure 2. Targeting Bitbow fluorescent proteins (FPs) to multiple subcellular compartments enables high-throughput lineage tracing without ambiguity. (a) The same Bitbow FPs are targeted to cell membrane, nucleus or Golgi apparatus to generate spectrally-spatially resolvable Bitbow codes. **(b)** Up to 32,767 unique mngBitbow codes can be generated can be presented as 3 groups of 5-digit 0/1s in correspondence with the expression status of mAmetrine (A), mTFP1 (T), mNeonGreen (G), mKO2 (O) and tdKatushka2 (K). **(c)** Experimental setup of generating heat-shock induced mngBitbow1.0 labeling and imaging. **(d)** Maximum intensity projection of a 3rd instar mngBitbow1.0 brain. Scale bar, 50µm. **(e**, **e')** Two confocal image slices corresponding to two different z positions in the boxed region in (**b**). Scale bar, 10µm. **(f)** 3 clusters marked in (**e**, **e'**) are assigned mngBitbow barcodes. Asterisks indicate the neuroblasts of each cluster. The arrowhead highlights an adjacent neuroblast labeled by a distinct mngBitbow code. **(g)** Simulation of Bitbow code collision in lineage mapping experiments. Dashed curve lines are simulations based on theoretical Bitbow code frequencies. Solid curve lines are simulations based on experimentally observed Bitbow code frequencies. Vertical dotted line corresponds to mapping all of the 200 lineages in a single adult *Drosophila* central brain. **(h)** Percentages of cell clusters that are uniquely labeled, or 2 of them, or >=3 of them are labeled by the same mnBitbow (286 clusters, 4 brains) or mngBitbow (577 clusters, 6 brains) codes in each brain. **(i)** Percentages of mnBitbow (N=80, 4 brains) or mngBitbow (N=240, 6 brains) codes that are expressed in 1, or 2, or >=3 clusters in each brain. Means and standard deviations (SD) are shown. **(j)** Monte Carlo simulations estimate the number of animals that are needed (y-axis) to sample all lineages at least once in animal brains that have given numbers of lineages (x-axis). Solid lines, means. Shaded lines, SD. HS, heat-shock. Img, imaging.

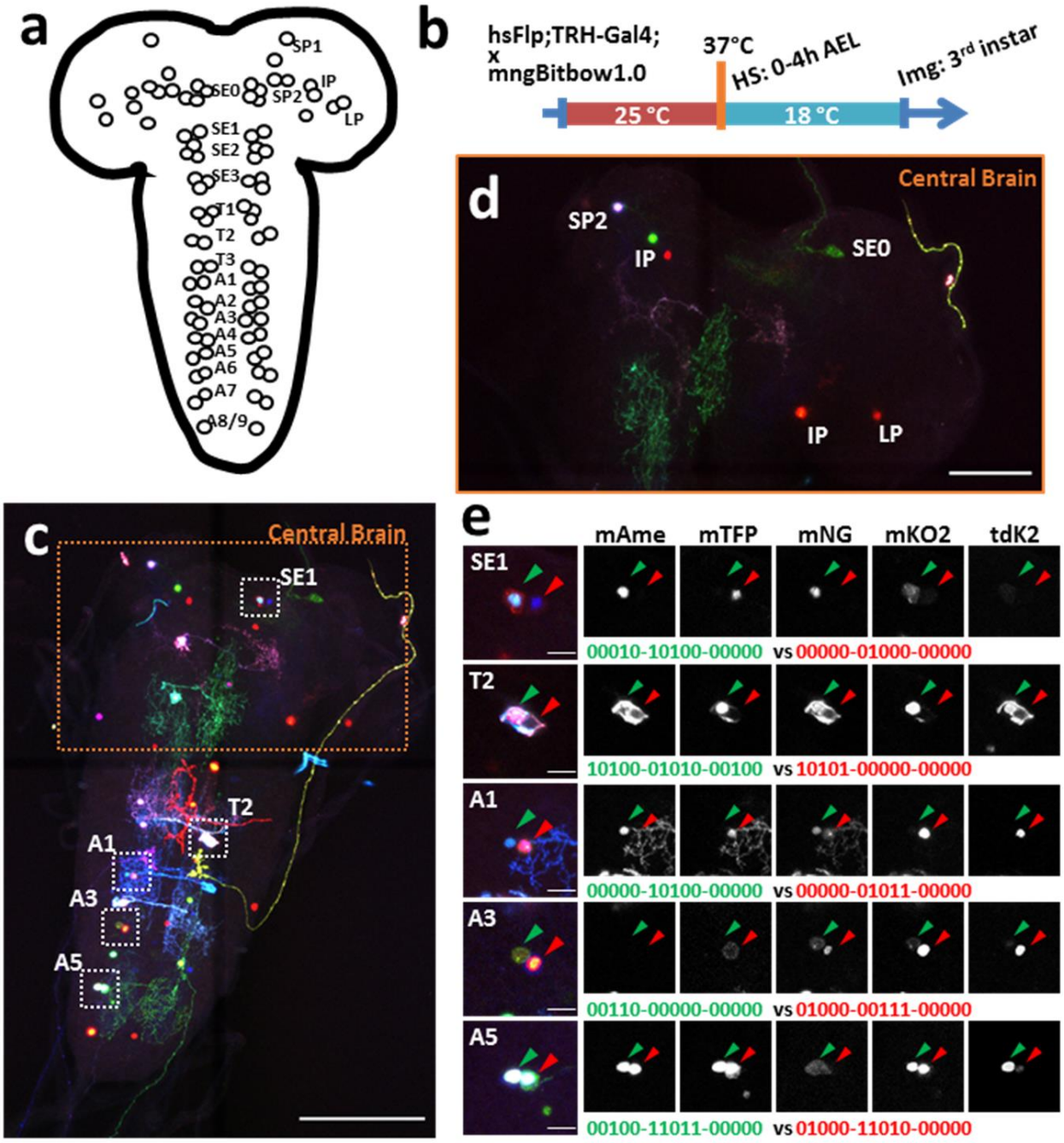
a
SP1
SE0
SP2
IP
LP
SE1
SE2
SE3
T1
T2
T3
A1
A2
A3
A4
A5
A6
A7
A8/9
b
hsFlp;TRH-Gal4;
x
mngBitbow1.0
37°C
HS: 0-4h AEL
Img: 3rd instar
25 °C
18 °C
d
Central Brain
SP2
IP
SE0
IP
LP
c
Central Brain
SE1
T2
A1
A3
A5
e
mAme
mTFP
mNG
mKO2
tdK2
SE1
00010-10100-00000 vs 00000-01000-00000
T2
10100-01010-00100 vs 10101-00000-00000
A1
00000-10100-00000 vs 00000-01011-00000
A3
00110-00000-00000 vs 01000-00111-00000
A5
00100-11011-00000 vs 01000-11010-00000

732

733 **Figure 3. Mapping the lineage relationships between clustered serotonergic neurons by**
734 **mngBitbow1.0. (a)** Schematic of clustered serotonergic neuron somas (circles) in the 3rd instar
735 brain. Neurons were named after their somas' locations in the central brain regions or VNC
736 segments. **(b)** Schematic of the experimental setup. **(c)** An example of mngBitbow1.0 labeled
737 serotonergic neurons in a 3rd instar larval brain. **(d)** Enlarged view of the central brain area in
738 (**c**). We found most of the serotonergic neurons were sparsely labeled in the central brain that
739 did not form clusters. Cell cluster identities are estimated based on relative cell body location.
740 **(e)** Enlarged boxed regions in (**c**) showed that pairs of serotonergic neurons in the same hemi-
741 segments could be easily found. mngBitbow codes in green and red correspond to neurons
742 marked by the green and red arrowheads, respectively. HS, heat-shock. Img, imaging. Scale
743 bars: (**c**, **d**) 100µm, (**e**) 10µm.

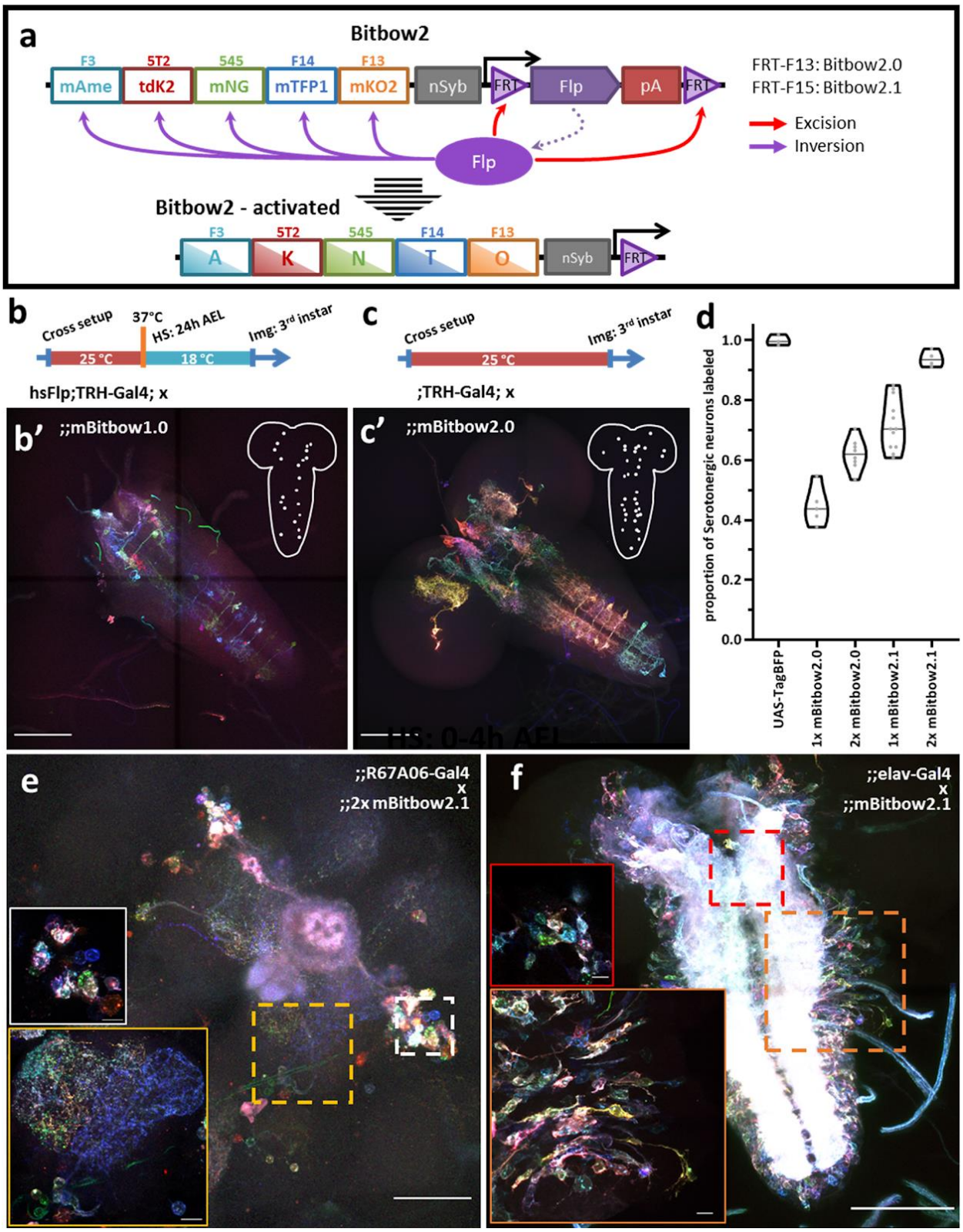
a
Bitbow2
F3
5T2
545
F14
F13
mAme
tdK2
mNG
mTFP1
mKO2
nSyb
FRT
Flp
pA
FRT
FRT-F13: Bitbow2.0
FRT-F15: Bitbow2.1
Excision
Inversion
Flp
Bitbow2 - activated
A
K
N
T
O
b
Cross setup
37°C
HS: 24h AEL
Img: 3rd instar
25 °C
18 °C
hsFlp;TRH-Gal4; x
b'
;;mBitbow1.0
c
Cross setup
Img: 3rd instar
25 °C
;TRH-Gal4; x
c'
;;mBitbow2.0
d
proportion of Serotonergic neurons labeled
1.0
0.8
0.6
0.4
0.2
0.0
UAS-TagBFP
1x mBitbow2.0
2x mBitbow2.0
1x mBitbow2.1
2x mBitbow2.1
e
;;R67A06-Gal4
x
;;2x mBitbow2.1
f
;;elav-Gal4
x
;;mBitbow2.1

744

745 **Figure 4. Bitbow2 enables broad neuron morphology labeling with a simple transgenic setup.**
746 **(a)** Schematic of Bitbow2 design. A self-regulating Flp module is added to ensure proper
747 transient Flp activity without the need of an additional cross to the heat-shock Flp fly. Flp
748 expression is driven by a neuron-specific n-Synaptobrevin (nSyb) promoter and terminated by
749 self-excising between the flanking FRT sites, which have lower efficiency compared to those
750 used in the Bitbow1 modules. This ensures proper Bitbow recombination before Flp self-
751 excision to reach a stable genetic outcome. Compared to a **(b)** Bitbow1 labeling experiment, a
752 **(c)** Bitbow2 labeling experiment requires only a direct cross to the TRH-Gal4 driver fly without
753 the need of heat-shock. **(b'**, **c')** indicate that mBitbow1.0 labeled fewer serotonergic neurons
754 than Bitbow2.0 does. Inserted schematics indicate the somas of the labeled serotonergic
755 neurons. **(d)** Quantification of the percentage of serotonergic neurons being labeled in different
756 Bitbow2 flies, normalized to the labeling of a UAS-TagBFP fly. Each dot that overlays on the
757 violin plots corresponds to the cell counting from one brain. **(e)** Adult neurons labeled in an
758 offspring of the 2x mBitbow2.1 fly crossed to the R67A06-Gal4 fly. White and yellow insets
759 show representative soma and neurite labeling, respectively. **(f)** Larva neurons labeled in an
760 offspring of the 2x mBitbow2.1 fly crossed to the elav-Gal4 fly. Red and orange insets show
761 neighboring neurons labeled in many distinct Bitbow colors in the central brain and in the VNC,
762 respectively. HS, heat-shock. Img, imaging. Scale bars: (**b'**, **c'**, **f**) 100µm, (**e**) 50µm, (**e**, **f** inserts)
763 10µm.

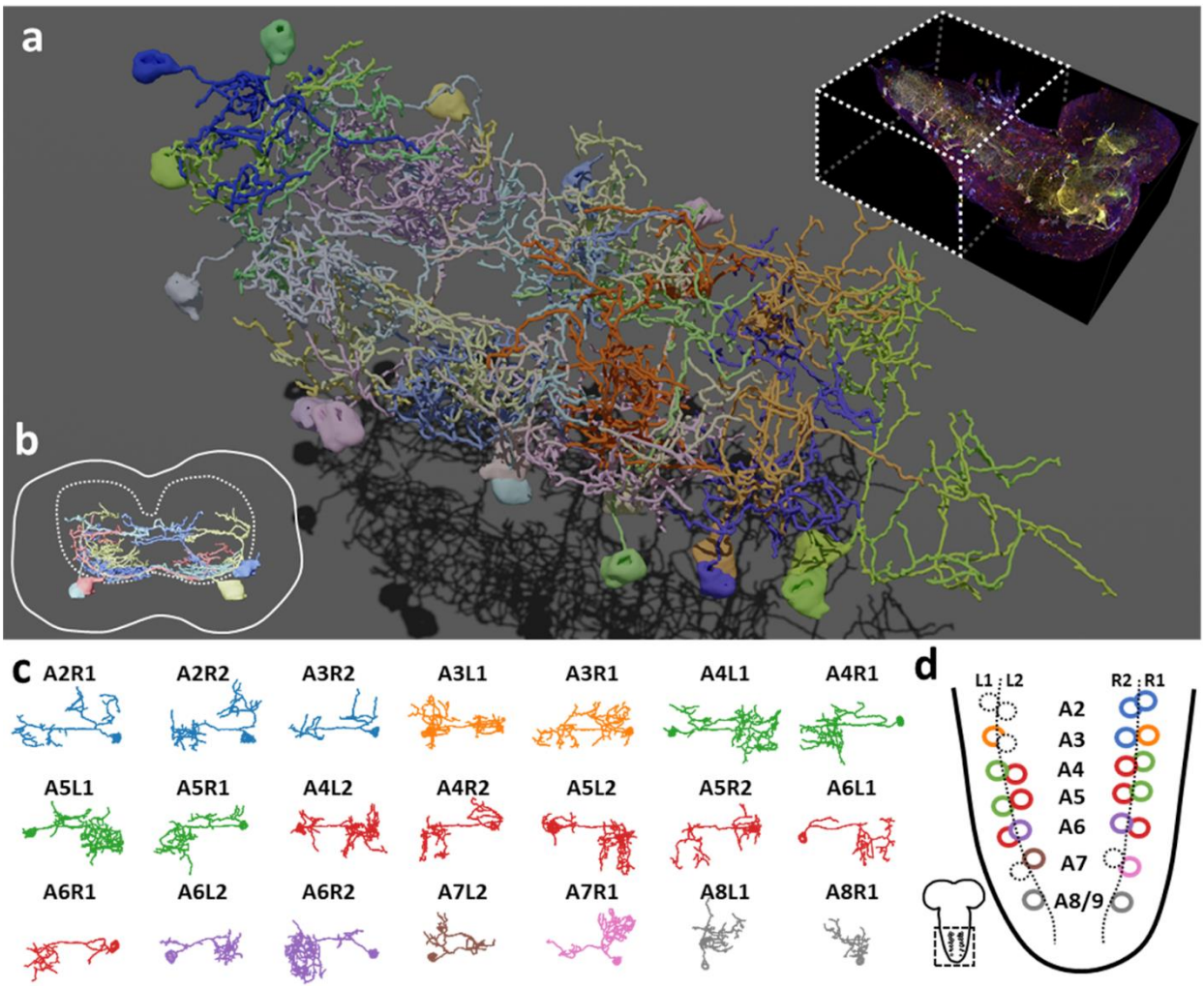
a
b
c
A2R1
A2R2
A3R2
A3L1
A3R1
A4L1
A4R1
A5L1
A5R1
A4L2
A4R2
A5L2
A5R2
A6L1
A6R1
A6L2
A6R2
A7L2
A7R1
A8L1
A8R1
d
L1
L2
R2
R1
A2
A3
A4
A5
A6
A7
A8/9

764

765 **Figure 5. Bitbow2 tracing enables serotonergic neuron morphology and network analysis in**
766 **larval VNC. (a)** 3D rendering of traced VNC serotonergic neurons labeled by Bitbow2 in a single
767 brain. Top right, dashed-line box indicates the VNC volume that has been traced. **(b)** Cross-
768 sectional view of the traced serotonergic neurons located in the A5 segment (solid outline),
769 which illustrates that the somas (solid oval shapes) are located at the very ventral part of the
770 VNS while the neurites occupy mostly in the sensory zone (ventral part) of the neuropil (dashed
771 outline). **(c)** Z-projections (dorsal view) of 21 traced serotonergic neurons categorized into 8
772 morphological subtypes that are indicated by distinct pseudo-colors. **(d)** Schematic of the
773 abdominal VNC and serotonergic neurons. Circles indicate the soma locations of the traced
774 serotonergic neurons, and their colors correspond to the morphological subtype pseudo-colors
775 in (**c**). Dashed circles indicate the soma locations of the unlabeled serotonergic neurons.